International Journal of Multiphase Flow 36 (2010) 127–134

Contents lists available at ScienceDirect

International Journal of Multiphase Flow

journal homepage: www.elsevier.com/locate/ijmulflow

Review

Direct numerical simulation of particulate flows with a fictitious domain method

Zhaosheng Yu *, Xueming Shao

Department of Mechanics, State Key Laboratory of Fluid Power Transmission and Control, Zhejiang University, 310027 Hangzhou, China

ARTICLE INFO

Article history:
Received 10 October 2008
Received in revised form 6 September 2009
Accepted 19 October 2009
Available online 27 October 2009

Keywords:
Fictitious domain
Particulate flows
Direct numerical simulation
Non-Newtonian
Non-isothermal

ABSTRACT

Our works on the fictitious domain method for the direct numerical simulation of particulate flows are reviewed, and particularly our recent progresses in the simulations of the motion of particles in Poiseuille flow at moderately high Reynolds numbers are reported. The method is briefly described, and its capability to simulate the motion of spherical and non-spherical particles in Newtonian, non-Newtonian and non-isothermal fluids is demonstrated. In addition, the applications of the fictitious domain method reported in the literature are also reviewed, and some comments on the features of the fictitious domain method and the immersed boundary method are given.

1. Introduction

Particulate flows are ubiquitous in nature and industrial applications. Dynamic simulation of the motion of particles in particulate flows is capable of providing both microscopic and macroscopic information and consequently has become an important investigative tool for multiphase flow problems. A variety of dynamic simulation methods for particulate flows have been proposed in the literature: the point-particle-approximation-based methods (Crowe et al., 1998), the low-Reynolds-number-theory-based methods such as Stokesian dynamics (Brady and Bossis, 1988), the boundary element method (e.g. Phan-Thien et al., 1991) and the slender-body theory (e.g. Lin et al., 2003), the force-coupling method (Lomholt et al., 2002; Lomholt and Maxey, 2003), the physalis method (Zhang and Prosperetti, 2005) and several other boundary-fitted and non-boundary-fitted methods. The typical boundary-fitted methods are the Arbitrary Lagrangian–Eulerian (ALE) finite element method (Hu et al., 1992, 2001; Hu, 1996) and the space–time finite element method (Johnson and Tezduyar, 1996). The non-boundary-fitted methods include the lattice Boltzmann method (e.g. Ladd, 1994; Ladd and Verberg, 2001; Aidun et al., 1998; Qi, 1999; Feng and Michaelides, 2005), the fictitious domain method (FD) (e.g. Glowinski et al., 1999, 2001; Patankar et al., 2000; Yu et al., 2004; Hwang et al., 2004; Sharma and Patankar, 2005; Veeramani et al., 2007; Yu and Shao, 2007), the immersed boundary (IB) method (e.g. Höfler and Schwarzer, 2000; Uhlmann, 2005; Kim and Choi, 2006; Wang et al., 2008), and the immersed interface method (e.g. Le et al., 2006; Xu and Wang, 2006). We note that the physalis method (Zhang and Prosperetti, 2005) is also a non-boundary-fitted method, but differs from others in that the general analytic solution of the Stokes equations is used in the particle boundary region to transfer the no-slip condition from the particle surface to the adjacent grid nodes and compute the hydrodynamic force on the particle. This technique has been shown to allow for accurate solution of particulate flows up to a particle Reynolds number of one hundred on coarse grids, and later adopted by Perrin and Hu (2008) in their explicit finite difference scheme. For the boundary-fitted methods, the fluid flow is computed on a boundary-fitted mesh and repeated re-meshing and solution projection is normally required as the interfaces move, whereas for the non-boundary-fitted methods, the fluid flow is computed on a stationary grid, thus eliminating the need for repeated re-meshing and projection (Joseph, 2002). As a result, the non-boundary-fitted methods are, generally speaking, simpler and more efficient than the boundary-fitted methods, in particular for the simulation of concentrated suspensions.

The fictitious domain (FD) method was initially developed to solve partial differential equations in a complex geometry, as pointed by Glowinski et al. (1999). Glowinski et al. (1994a,b, 1995, 1997) described the FD methods for the Dirichlet problem in which the boundary condition is enforced with the Lagrange multiplier method, and they employed the methods to solve some differential equations and the incompressible viscous unsteady flows in complex or moving geometries. The Lagrange multiplier based FD method was also used by Bertrand et al. (1997) and Tanguy et al. (1996) to calculate the three-dimensional Stokes flows of Newtonian and viscoplastic fluids in a mixer. Glowinski et al.

* Corresponding author. Tel.: +86 571 87951768; fax: +86 571 87951464.
E-mail address: yuzhaosheng@zju.edu.cn (Z. Yu).

0301-9322/$ - see front matter © 2009 Elsevier Ltd. All rights reserved.
doi:10.1016/j.ijmultiphaseflow.2009.10.001

(1999) developed the distributed Lagrange multiplier based FD method (DLM/FD) to simulate particulate flows where the rigid particles move freely. The key idea in this method is that the interior domains of the particles are filled with the same fluids as the surroundings and the Lagrange multiplier (i.e. a pseudo body force) is introduced to enforce the interior (fictitious) fluids to satisfy the constraint of rigid-body motion (Glowinski et al., 1999). In the DLM/FD code of Glowinski et al. (2001), the finite element method was used to solve the fluid equations, and a twice-coarser pressure element with respect to the velocity element was adopted. Patankar et al. (2000) proposed a version of the DLM/FD technique that imposed the deformation rate tensor in the particle domain equal to zero. Patankar (2001) developed a fast computation technique in which the flow fields were solved with a finite difference method and the velocities of particle were obtained explicitly without iteration. This approach was later published by Sharma and Patankar (2005). Yu et al. (2002) substituted the Q1-P0 finite element method for the twice-coarser pressure element based one, and Yu et al. (2004) further replaced the Q1-P0 finite element method with a half-staggered finite difference method for the solution of the flow fields. Hwang et al. (2004) proposed a DLM/FD method for the simulation of particle motion in a sliding bi-periodic box at low Reynolds numbers. Unlike other versions, where the DLM is distributed in the solid domain and the operator-splitting scheme is adopted to simplify the computations, in the code of Hwang et al., the DLM is distributed only on the particle boundary, and the whole system is solved all together which eliminates the splitting error but increases the computational cost substantially. Sharma and Patankar (2004) proposed an iterative DLM scheme which is suitable for low *Re* or quasi-Stokes simulations, and they applied this approach to the simulation of Brownian motion of particles. Veeramani et al. (2007) and Yu and Shao (2007) developed the non-iterative DLM/FD schemes in which the particle velocities and the pseudo body force (Lagrange multiplier) were obtained explicitly, as in Sharma and Patankar (2005), but the derived expressions for the particle velocities and the computational schemes for the flow problem were different for these three methods. The fictitious domain method has been applied to various particulate flows such as the sedimentation of 6400 circular particles in a two-dimensional cavity in the Rayleigh–Taylor instability (Pan et al., 2001), the fluidization of a bed of 1024 spherical particles (Pan et al., 2002), the sedimentation of a spherical particle in a vertical tube (Yu et al., 2004), the sedimentation of two spheroids (Pan et al., 2005), the pattern formation of a rotating suspension of non-Brownian settling particles in a fully filled cylinder (Pan et al., 2007), the sedimentation of circular particles in viscoelastic fluids (Singh et al., 2000; Yu et al., 2002), the sedimentation of spherical particles in viscoelastic fluids (Singh and Joseph, 2000), shear-thinning fluids (Yu et al., 2006a) and Bingham fluids (Yu and Wachs, 2007), the inertia-induced migration in a plane Poiseuille flow (Pan and Glowinski, 2002) and a circular Poiseuille flow (Yu et al., 2004; Pan and Glowinski, 2005; Shao et al., 2008), the particle motion in a sliding bi-periodic frame (Hwang et al., 2004) and a planar elongational flow (Hwang and Hulsen, 2006), flow-induced crystallization of particle-filled polymers (Hwang et al., 2006), the rotation of a spheroid in a Couette flow (Yu et al., 2007a) and a pipe flow (Pan et al., 2008), the shear-induced migration in a 2D circular Couette flow (Yu et al., 2007b), the heat transfer between particles and fluids (Yu et al., 2006b), the motion of floating particles (Singh and Joseph, 2005), and the electrophoresis of particles (Kadaksham et al., 2004). We note that the DLM/FD method has been extended by Baaijens (2001) and Yu (2005) to handle the fluid/elastic–structure interactions.

Compared to the lattice Boltzmann method, the DLM/FD method has an advantage of flexibility in the sense that it can be easily extended to any phenomenological equations such as the Poisson equation and the constitutive equations for a complex or non-Newtonian fluid whereas the extension of the lattice Boltzmann method to a complex fluid or the Poisson equation is much more involved.

There is no essential difference between the so-called fictitious domain and immersed boundary methods particularly for the fluid–particle (or structure) interaction problem since both terms of 'fictitious domain' and 'immersed boundary' refer to the non-boundary-fitted feature of the methods and any solid body has both volume (fictitious domain) and boundary (immersed). The non-boundary-fitted methods can be classified into two families: the body-force-based methods and non-body-force-based methods, depending on whether or not a pseudo body force (or momentum forcing) is introduced into the fluid momentum equations to enforce the rigid-body motion constraint in the particle domain or the no-slip condition on the particle boundary. All FD methods mentioned above are the body-force-based methods. In the original DLM/FD methods, the Lagrange multiplier is determined implicitly from the rigid-body motion constraint and solved together with the particle and fluid velocities. However, the Lagrange multiplier can also be calculated explicitly from the fractional-step time scheme and some reasonable approximations, and it appears to lose its original sense of the Lagrange multiplier (Patankar, 2001; Sharma and Patankar, 2005; Veeramani et al., 2007; Yu and Shao, 2007). The IB methods reported in the literature have body-force-based and non-body-force-based versions. In the body-force-based version, the body force is calculated explicitly from the spring force scheme (Peskin, 2002; Höfler and Schwarzer, 2000) or the direct-forcing scheme (Uhlmann, 2005; Kim and Choi, 2006). Many non-body-force-based IB methods have been proposed for the solution of the flow in a complex geometry (Mittal and Iaccarino, 2005), and in principle, these methods can be directly applied to the fluid–particle interactions since the hydrodynamic forces on the particles can be computed with the resolved flow fields. However, the body-force-based FD or IB methods have been predominately used for the particulate flows. A probable reason is: the hydrodynamic forces on the particles are of most importance to the simulation of the particulate suspensions, and it is difficult to obtain the accurate hydrodynamic forces via the computation of the fluid stress on the particle boundary for the non-body-force-based IB methods unless fine mesh is used, whereas for the body-force-based FD or IB method the hydrodynamic forces can be determined from the integration of the pseudo body force with reasonable accuracy even for coarse mesh, and furthermore the explicit computation of the hydrodynamic forces is normally not required to determine the particle velocities, which might be helpful to the robustness of the methods (Glowinski et al., 1999).

The primary aim of the present paper is to review our works on the FD method. The rest of the paper is organized as follows: In Section 2, we describe briefly our direct-forcing fictitious domain (DF/FD) method. In Section 3, we present a review of the applications of our FD codes and some validations. The conclusions are given in the final section.

2. Fictitious domain method

2.1. FD formulation

The DF/FD method is an improved version of our previous DLM/FD code. The DF/FD code is more efficient than the DLM/FD code since the Lagrange multiplier and the particle velocities are obtained without iteration, and it has been demonstrated that the DF/FD method is equally accurate and robust as the DLM/FD method (Yu and Shao, 2007). We briefly describe the DF/FD method in

the following, and more details on the method is referred to Yu and Shao (2007).

For simplicity of description, we will consider only one particle in the following exposition. Suppose that the particle density, volume and moment of inertia tensor, translational velocity, and angular velocity is ρ_s, V_p, $\mathbf{J}$, $\mathbf{U}$, and $\boldsymbol{\omega}_s$, respectively. The fluid viscosity and density is μ and ρ_f, respectively. Let $P(t)$ represent the solid domain, and Ω the entire domain including interior and exterior of the solid body. By introducing the following scales for the non-dimensionlization: L_c for length, U_c for velocity, L_c/U_c for time, $\rho_f U_c^2$ for the pressure, and $\rho_f U_c^2/L_c$ for the pseudo body force, the dimensionless FD formulation in strong form for the incompressible fluid can be written as follows:

$$\frac{\partial \mathbf{u}}{\partial t} + \mathbf{u}\cdot\nabla\mathbf{u} = \frac{\nabla^2\mathbf{u}}{Re} - \nabla p + \lambda, \quad \text{in } \Omega, \tag{1}$$

$$\mathbf{u} = \mathbf{U} + \boldsymbol{\omega}_s \times \mathbf{r}, \quad \text{in } P(t), \tag{2}$$

$$\nabla\cdot\mathbf{u} = 0,, \tag{3}$$

$$(\rho_r - 1)V_p^*\left(\frac{d\mathbf{U}}{dt} - Fr\frac{\mathbf{g}}{g}\right) = -\int_P \lambda d\mathbf{x}, \tag{4}$$

$$(\rho_r - 1)\frac{d(\mathbf{J}^*\cdot\boldsymbol{\omega}_s)}{dt} = -\int_P \mathbf{r}\times\lambda d\mathbf{x}. \tag{5}$$

In the above equations, $\mathbf{u}$, p, $\boldsymbol{\lambda}$, and $\mathbf{r}$ are, respectively, the fluid velocity, the fluid pressure, the pseudo body force that is defined in the solid domain, and the position vector with respect to the particle mass center. ρ_r denotes the particle–fluid density ratio, Re the Reynolds number defined by $Re = \rho_f U_c L_c/\mu$, Fr the Froude number defined by $Fr = gL_c/U_c^2$, V_p^* the dimensionless particle volume (area in case of two-dimensions) defined by $V_p^* = V_p/L_c^d$ (d being the dimensionality of the problem), and $\mathbf{J}^*$ the dimensionless moment of inertia tensor defined by $\mathbf{J}^* = \mathbf{J}/(\rho_s L_c^{d+2})$ The weak formulation of (1)–(5) was derived by Glowinski et al. (1999).

2.2. Numerical schemes

A fractional-step time scheme is used to decouple the system (1)–(5) into the following two sub-problems.

Fluid sub-problem for $\mathbf{u}^*$, p:

$$\frac{\mathbf{u}^* - \mathbf{u}^n}{\Delta t} - \frac{\nabla^2\mathbf{u}^*}{2Re} = -\nabla p - \frac{1}{2}\left[3(\mathbf{u}\cdot\nabla\mathbf{u})^n - (\mathbf{u}\cdot\nabla\mathbf{u})^{n-1}\right] + \frac{\nabla^2\mathbf{u}^n}{2Re} + \lambda^n, \tag{6}$$

$$\nabla\cdot\mathbf{u}^* = 0. \tag{7}$$

A finite-difference-based projection method on a homogeneous half-staggered grid is used for the solution of the above fluid equations (6) and (7). The diffusion problem (6) can be decomposed into tri-diagonal systems with the ADI technique and the Poisson equation for the pressure arising from the projection scheme is solved with the FFT-based fast solver. All spatial derivatives are discretized with the second-order central difference scheme.

Particle sub-problem for $\mathbf{U}^{n+1}$, $\boldsymbol{\omega}^{n+1}$:

$$\rho_r V_p^*\frac{\mathbf{U}^{n+1}}{\Delta t} = (\rho_r - 1)V_p^*\left(\frac{\mathbf{U}^n}{\Delta t} + Fr\frac{\mathbf{g}}{g}\right) + \int_P\left(\frac{\mathbf{u}^*}{\Delta t} - \lambda^n\right)d\mathbf{x}, \tag{8}$$

$$\rho_r\frac{\mathbf{J}^*\cdot\boldsymbol{\omega}^{n+1}}{\Delta t} = (\rho_r - 1)\left[\frac{\mathbf{J}^*\cdot\boldsymbol{\omega}_s^n}{\Delta t} - \boldsymbol{\omega}_s^n\times(\mathbf{J}^*\cdot\boldsymbol{\omega}_s^n)\right] + \int_P r\times\left(\frac{\mathbf{u}^*}{\Delta t} - \lambda^n\right)d\mathbf{x}. \tag{9}$$

Note that the above equations have been re-formulated so that all the right-hand side terms are known quantities and consequently the particle velocities $\mathbf{U}^{n+1}$ and $\boldsymbol{\omega}^{n+1}$ are obtained without iteration, unlike the original DLM/FD method.

Then, $\boldsymbol{\lambda}^{n+1}$ defined at the Lagrangian nodes are determined from:

$$\boldsymbol{\lambda}^{n+1} = \frac{\mathbf{U}^{n+1} + \boldsymbol{\omega}_s^{n+1}\times\mathbf{r} - \mathbf{u}^*}{\Delta t} + \boldsymbol{\lambda}^n, \tag{10}$$

and the fluid velocities $\mathbf{u}^{n+1}$ at the Eulerian nodes are obtained from:

$$\mathbf{u}^{n+1} = \mathbf{u}^* + \Delta t(\boldsymbol{\lambda}^{n+1} - \boldsymbol{\lambda}^n). \tag{11}$$

In the above manipulations, the bi-linear (or tri-linear) function is used to interpolate the fluid velocity from the Eulerian nodes to the Lagrangian nodes, and to distribute the pseudo body force from the Lagrangian nodes to the Eulerian nodes. The arrangements of Lagrangian points for circular, spherical and spheroidal particles are depicted in Fig. 1. The Lagrangian (collocation) points are also used to compute the integral terms in (8) and (9) and the moment of inertia tensor (and possibly the mass center for particles of unsymmetrical shape).

The artificial repulsive force collision model (Glowinski et al., 1999), the lubrication model (Sierou and Brady, 2001) and the hard-sphere collision model (Crowe et al., 1998) have been implemented in our code (Yu et al., 2002, 2006b; Shao et al., 2008) to prevent the mutual penetration of particles. We notice that Ardekani and Rangel (2008), Ardekani et al. (2008), and Wachs (2009) have recently proposed nice collision schemes for their FD simulations.

The reader is referred to Yu and Shao (2007) for the scheme for the non-spherical particles, Yu et al. (2006a) for the thixotropic shear-thinning and viscoelastic fluids, Yu and Wachs (2007) for the Bingham fluids, and Yu et al. (2006b) for the non-isothermal fluids.

3. Validations and applications

3.1. Particle motion in Newtonian fluids

In Yu et al. (2004), the sedimentation of a sphere and its radial migration in a Poiseuille flow in a vertical tube filled with a Newtonian fluid were simulated with the DLM/FD code. The flow features, the settling velocities, the trajectories and the angular velocities of the spheres settling in a tube at different Reynolds numbers were presented. The radial, angular and axial velocities of both neutrally buoyant and non-neutrally buoyant spheres in a circular Poiseuille flow were reported for the tube Reynolds number up to 300. The results were in remarkably good agreement with the available experimental data.

In Shao et al. (2008), the inertial migration of neutrally-buoyant spherical particles in a circular Poiseuille flow was numerically

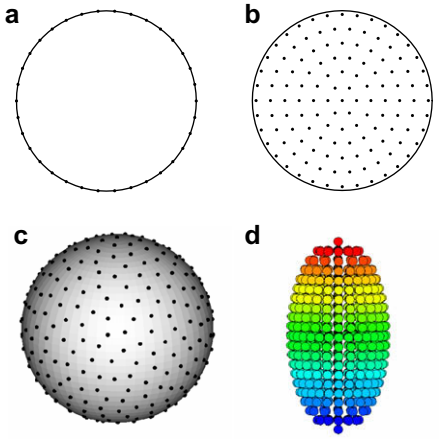

Fig. 1. Arrangements of Lagrangian points in cases of (a) a 2D cylinder with the no-slip condition enforced only on the boundary, (b) a circular particle, (c) a spherical particle (only the points on one layer is shown), and (d) a prolate spheroid. From Yu and Shao (2007).

investigated for the tube Reynolds number up to 2200 with the DF/FD code. Inner equilibrium positions were observed as the Reynolds number exceeded a critical value, in qualitatively agreement with the previous experimental observations (Matas et al., 2004). The results indicated that the pipe length had a significant effect on the equilibrium position of the particle, and the particle could stay stably in the vicinity of the pipe wall at a higher Reynolds number in a shorter pipe. In addition, the particle was observed to induce stable mirror-symmetric structures, characterized by the velocity streaks and secondary flows, similar to the traveling-wave solution found in pipe flow (Pringle and Kerswell, 2007). The particle-induced structures appeared stronger in a longer pipe probably due to the fact that the secondary flows at upstream and downstream of a particle were directed oppositely and thus could be suppressed at a small distance between the consecutive particles, therefore, one could assume that the particle-induced structures served to push the particle away from the pipe wall in a longer pipe.

Shao et al. (2008) observed that there existed two branches of stable equilibrium positions at the particle–pipe radius ratio a/R being 0.15 and the pipe length being 2, as shown in Fig. 2. The particle migrated to the outer Segré–Silberberg branch at Re smaller than Re_{c1} (around 1000), and to the inner one at Re larger than Re_{c2} (around 1300), irrespective of its initial position. For $Re_{c1} \leqslant Re \leqslant Re_{c2}$, the particle migrated to either the outer one or the inner one, depending on its initial position. The above results indicate that there existed an unstable branch of equilibrium positions (i.e., zero lift force) connecting the two stable ones for $Re_{c1} \leqslant Re \leqslant Rec2$. We note that a similar turning point bifurcation behavior was previously observed for a non-zero lift force on a circular particle (or the lift-off position of a heavier particle) in a plane Poiseuille flow by Patankar et al. (2001).

The inertial migration of a single neutrally-buoyant circular particle in both non-oscillatory and oscillatory pressure-driven flows in a 2D channel at moderately high Reynolds numbers has been numerically investigated in Sun et al. (2009). In both non-oscillatory and oscillatory cases, there was only one equilibrium position for any Reynolds number, and the equilibrium positions first shift closer to the channel wall and then closer to the channel centerline as the Reynolds number increases. The equilibrium positions for a spherical particle in a 3D non-oscillatory channel flow were also computed and found to behave in the same way as the 2D case, as shown in Fig. 2. The reason for the difference in the equilibrium positions between the channel and pipe flows was attributed to the effects of the outer boundary on the particle-induced flow structures. The oscillatory flow generally made the equilibrium position closer to the channel centerline, and the equilibrium positions were more sensitive to the frequency than the amplitude of the oscillatory pressure gradient.

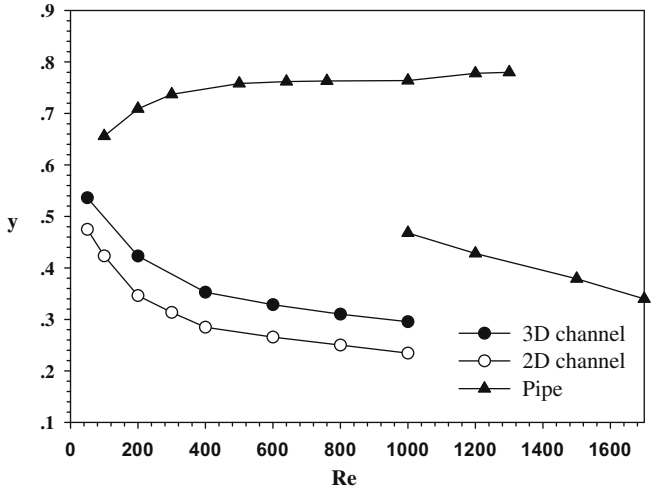

Fig. 2. Comparison of lateral equilibrium positions of neutrally-buoyant particles in the 2D and 3D channels, and the pipe at different Reynolds numbers. $a/H = 0.15$, $L/H = 2$ (H being half channel height) for the channel case and $a/R = 0.15$, $L/R = 2$ for the pipe case. From Sun et al. (2009).

We have recently simulated the particle-laden pipe flow at the Reynolds number ranging from 1500 to 3500, in an attempt to reveal the mechanism by which particles trigger the turbulence transition, as observed by Matas et al. (2003). The periodic boundary condition is introduced in the streamwise direction and the pressure gradient is fixed to be constant. We take the tube radius and the maximum velocity of initial laminar flow as the characteristic length and velocity, respectively. Fig. 3 shows the velocity fields in the streamwise plane passing through the particle center at different times for (Re, a/R, L/R) = (1500, 0.1, 4). The results indicate that in the $L = 4R$ pipe the flow structure induced by the particle of $a/R = 0.1$ loses stability at $Re = 1500$, namely, the intensity of streamwise vortices increases rapidly and the flow becomes turbulence (Fig. 3b–d). The motion of the particle is dominated by the streamwise vortices at turbulence stage. The flow relaminarizes subsequently, and the particle migrates to the equilibrium position again (Fig. 3e). The particle then can trigger another round of the flow instability, till the system eventually reaches a stable state: the particle spirals forward along the tube wall, accompanied by a stable flow structure, as shown in Fig. 3f. More results, including those for higher Reynolds numbers, multiple particles and larger particles will be reported in another paper.

3.2. Particle motion in non-Newtonian fluids

Yu et al. (2002) investigated the aggregation of circular particles settling in a viscoelastic fluid with the proposed DLM/FD method and found that the asymmetric distribution of the second normal stress due to the rotation of the particle was responsible for the aggregation of two side-by-side settling particles and the attraction of a particle toward the wall.

Yu et al. (2006a) proposed a DLM/FD method for the particle motion in a thixotropic shear-thinning fluid. The accuracy of the method was validated by comparing the computed drag coefficients for a sphere settling in a tube filled with a power-law fluid at low Reynolds numbers to the results of Missirlis et al. (2001) who used a boundary-fitted finite element method. In the DLM/FD computations, two mesh resolutions were used: $h = a/4$ and $h = a/8$. The maximum relative error in the results presented in Fig. 4 is around 4%. The accuracy of the proposed method, as a simple non-boundary-fitted method, is satisfactory. The method was then used to examine the aggregation of particles settling in a thixotropic shear-thinning fluid. The results confirmed that the memory of shear-thinning was responsible for the aggregation of two end-to-end settling particles, and indicated that the elasticity of the fluid, though may be weak, seemed necessary for the randomly distributed particles to aggregate into stable clusters or columns.

In Yu and Wachs (2007), a fictitious domain method for the dynamic simulation of particle motion in a Bingham viscoplastic fluid was proposed. The method was verified by comparing the results on the lid-driven cavity flow, the drag coefficient for a sphere settling in a tube and the hydrodynamic interactions between two spheres translating along the tube axis to the data available in the literature. The computations confirmed that the drag coefficient for a sphere settling in a Bingham fluid at non-zero Reynolds numbers can be well correlated with an effective Reynolds number. For two approaching spheres, there existed a critical separation distance above which a drag-reduction was observed and

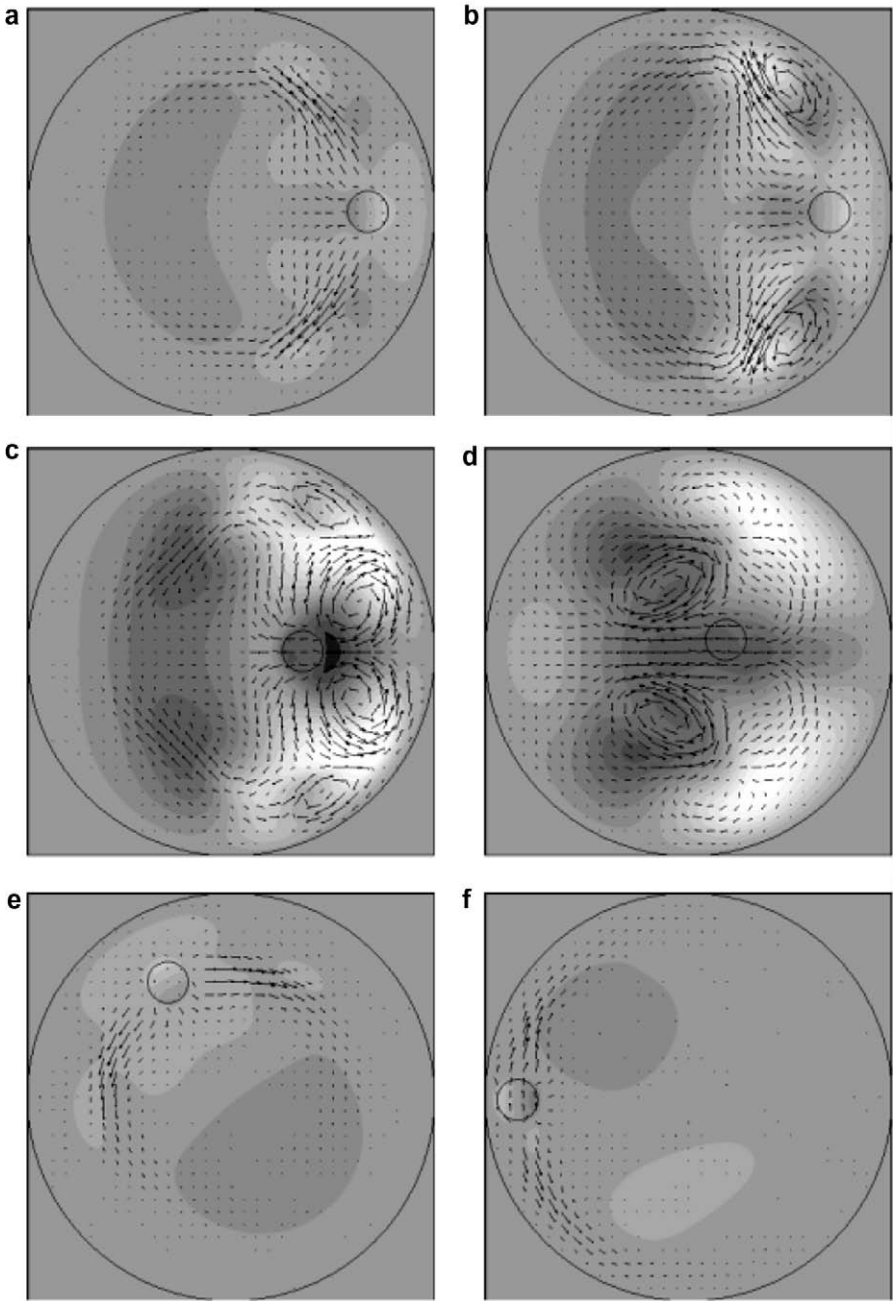

Fig. 3. Velocity fields in the particle plane for the pipe flow at different times (a) $t = 100$; (b)$t = 125$; (c) $t = 150$; (d) $t = 200$; (e) $t = 900$; (f) $t = 2250$. $(Re, a/R, L/R) = (1500, 0.1, 4)$. The contours (grayscale) indicate the streamwise velocity relative to the parabolic profile with minimum (darkest) and maximum levels and the increment are −0.22, 0.26, and 0.04, respectively.

below which a drag-enhancement took place, compared to the drag for a single sphere. These observations were explained by a consideration of the competition between a shear-thinning plastic force and a repulsive lubrication force on the sphere occurring in the squeezing flow.

3.3. Particle motion in non-isothermal fluids

In Yu et al. (2006b), the DLM/FD method was extended to deal with heat transfer in particulate flows in two dimensions. The Boussinesq approximation was employed for the coupling between the flow and temperature fields. The code for the case of fixed temperature on the immersed boundary was verified by comparing favorably the results on the natural convection driven by a hot cylinder eccentrically placed in a square box and on the sedimentation of a cold circular particle in a vertical channel to the data in the literature. The code for the case of freely varying temperature on the boundaries of freely moving particles was applied to analyze the motion of a catalyst particle in a box and in particular the heat conductivities of nanofluids and sheared non-colloidal suspensions, respectively. The preliminary computational results supported the argument that the micro-heat-convection in the fluids is primarily responsible for the unusually high heat conductivity of nanofluids.

We have recently applied the method to examine the interactions between the particle sedimentation and the natural convec-

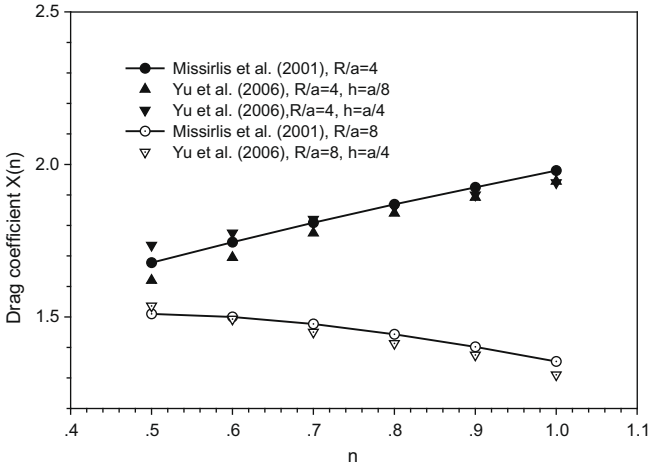

Fig. 4. Comparison between the drag coefficients for a sphere settling in a tube filled with a power-law fluid as a function of the power-law index at low Reynolds numbers. From Yu et al. (2006a).

tion in a square box due to heating from the bottom plate, inspired by the experimental work of Chen et al. (2005). In our simulations, the width of the box is 64d, d being the particle diameter. The dimensionless temperature is zero on the top boundary, and unity on middle one third of the bottom boundary. The adiabatic condition is imposed on the remaining boundaries. The heat flux is conserved across the particle/fluid interface. We take the particle diameter as the characteristic length, and the settling velocity of a single particle in a vertical channel of 64d width at vanishing Reynolds numbers as the characteristic velocity, i.e.,

$$U_c = \frac{d^2}{16K\mu}(\rho_s - \rho_f)g, \tag{12}$$

in which K is a constant related to the effect of the channel width on the drag force and can be expressed in terms of the ratio of the channel width to the particle diameter W^* (i.e., W/d) (Happel and Brenner, 1965):

$$K = \frac{1}{\ln(W^*) - 0.9157 + 1.7244/(W^*)^2 - 1.7302/(W^*)^4 + 2.4056/(W^*)^6 - 4.5913/(W^*)^8}.$$

We fix the Grashof number (based on the particle diameter) $Gr = 0.25$, the density ratio $\rho_r = 1.2$, the heat capacity ratio $c_{pr} = 0.50$, the heat conductivity ratio $k_r = 5$, the heat expansion ratio $\beta_r = 0$ (i.e., the particle density variation is not considered). Then the relative importance of the sedimentation to the natural convection is determined by the Reynolds number and the Prandtl number, since the Reynolds number is based on the sedimentation rate and the intensity of natural convection depends on the Rayleigh number which is defined by $Ra = GrPr$ (Pr denotes the Prandtl number). The particles are randomly distributed in the box at initial time. Mesh size $h = d/16$ and time step $\Delta t = 0.001$ are used.

Fig. 5 shows the isotherms and velocity fields for 200 circular particles at $t = 50$ in two cases: (Re, Pr) = (0.02, 250), and (Re, Pr) = (0.4, 10). In the former case, the natural convection is strong and predominates over the sedimentation of the particles. The maximum rising velocity of the fluids at $t = 50$ is 7.6, and some particles are entrained upwards by the heat plume. For the latter case, the maximum rising velocity of the fluids at $t = 50$ is 1.74, and the sedimentation of the particles predominates over the weak natural convection.

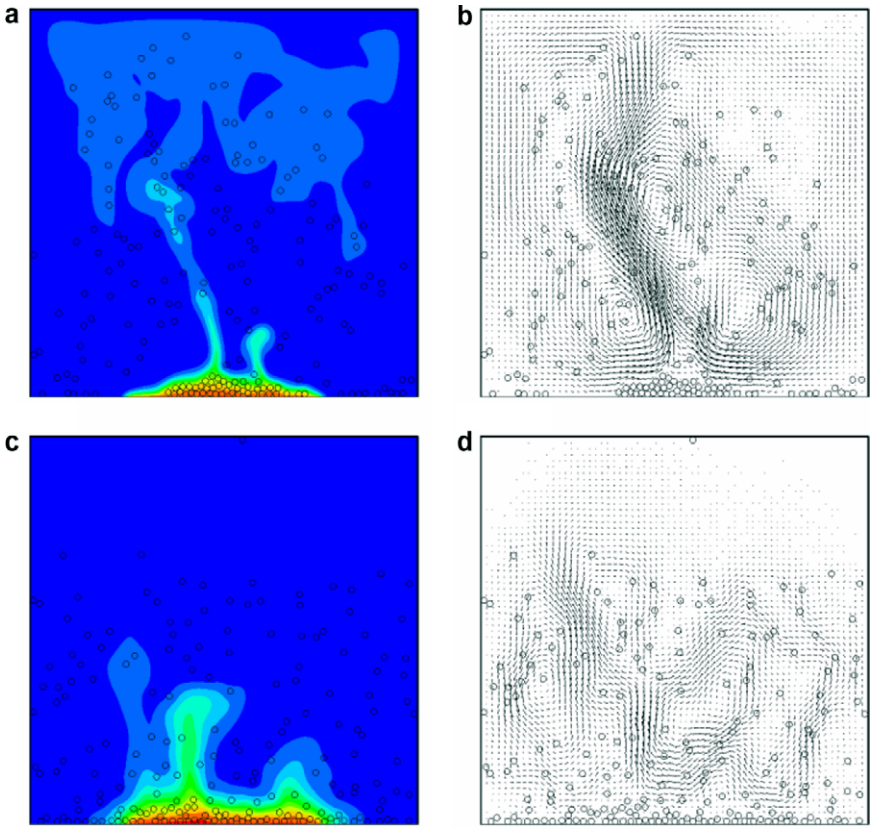

Fig. 5. Isotherms (a and c) and velocity fields (b and d) for the sedimentation of 200 circular particles in a 64d × 64d square box heated at the bottom for (a and b) $Re = 0.02$, $Pr = 250$, and (c and d) $Re = 0.4$, $Pr = 10$. For other parameters, $Gr = 0.25$, $k_r = 5$, $c_{pr} = 0.50$, $\beta_r = 0$, and $\rho_r = 1.2$.

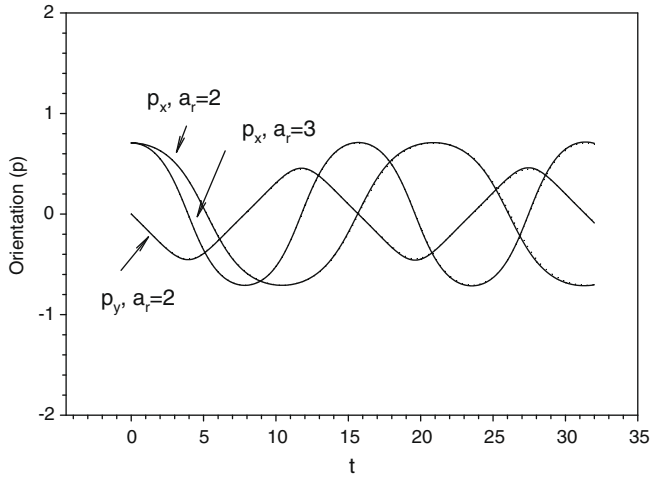

Fig. 6. Comparison between the calculated orientation and the analytical Jeffery orbit for a prolate spheroid in simple shear flow at a low Reynolds number. Solid lines: our results; dotted lines: analytical results, the two being in excellent agreement. From Yu and Shao (2007).

3.4. Non-spherical particles

We take the rotation of a spheroid in a Couette flow at low Reynolds numbers as a test problem. The comparison between the orientation of the spheroid calculated with DF/FD method and the analytical Jeffery orbits for the spheroid aspect ratio $a_r = 2$ and 3 is shown in Fig. 6. p_x and p_y are the x and y components of the unit orientation vector along the symmetric axis of the spheroid, respectively. The numerical and analytical results are in remarkably good agreement with each other.

In Yu et al. (2007a), the rotation of a spheroid in a Couette flow at moderately high Reynolds numbers was numerically simulated with the fictitious domain method. The study was focused on the effects of inertia on the orbital behavior of prolate and oblate spheroids. The numerical orbits were found to be well described by a simple empirical model, which states that the rate of the spheroid rotation about the vorticity axis is a sinusoidal function of the corresponding projection angle in the flow-gradient plane, and that the exponential growth rate of the orbit function is a constant. The following transitions in the steady state with increasing Reynolds number were identified: Jeffery orbit, tumbling, quasi-Jeffery orbit, log rolling, and inclined rolling for a prolate spheroid; and Jeffery orbit, log rolling, inclined rolling, and motionless state for an oblate spheroid.

4. Conclusion

We have briefly reviewed the fictitious domain methods for the dynamic and direct simulations of particulate flows. Our DF/FD method has been briefly described. Its capability to simulate the motion of spherical and non-spherical particles in Newtonian, non-Newtonian and non-isothermal fluids has been demonstrated, and the main results from applications of our FD codes have been summarized.

Our FD code is very efficient for particulate flows due to the use of the fractional-step time scheme and a sequence of efficient solvers such as the finite-difference-based projection method for the Navier–Stokes equations, the FFT-based fast solver for the pressure Poisson equation, the ADI scheme for the velocity diffusion equation, and the non-iterative scheme for the rigidity constraints. However, the code is less efficient or accurate for the case of very low Reynolds numbers because of the use of the fractional-step time scheme, and the cases of the sedimentation at high particle Reynolds numbers (e.g. in hundreds), the viscoplastic flow at high Bingham numbers, and the viscoelastic flow at high Deborah numbers because the employed homogeneous non-boundary-fitted mesh cannot handle well the very thin boundary layer of the velocity or the polymer stress.

Acknowledgements

The authors gratefully acknowledge the financial support from the National Natural Science Foundation of China (Nos. 10602051 and 10872181) and the Major Program of the National Natural Science Foundation of China (No. 10632070).

References

Aidun, C.K., Lu, Y., Ding, E.-J., 1998. Direct analysis of particulate suspensions with inertia using the discrete Boltzmann equation. J. Fluid Mech. 373, 287–311.
Ardekani, A.M., Rangel, R.H., 2008. Numerical investigation of particle–particle and particle–wall collisions in a viscous fluid. J. Fluid Mech. 596, 437–466.
Ardekani, A.M., Dabiri, S., Rangel, R.H., 2008. Collision of multi-particle and general shape objects in a viscous fluid. J. Comput. Phys. 227, 10094–10107.
Baaijens, F.P.T., 2001. A fictitious domain/mortar element method for fluid–structure interaction. Int. J. Numer. Methods Fluids 35, 743–761.
Bertrand, F., Tanguy, P.A., Thibault, F., 1997. A three-dimensional fictitious domain method for incompressible fluid flow problems. Int. J. Numer. Methods Fluids 25, 719–736.
Brady, J.F., Bossis, G., 1988. Stokesian dynamics. Annu. Rev. Fluid Mech. 20, 111–157.
Chen, B., Mikami, F., Nishikawa, N., 2005. Experimental studies on transient features of natural convection in particles suspensions. Int. J. Heat Mass Transfer 48, 2933–2942.
Crowe, C., Sommerfeld, M., Tsuji, Y., 1998. Multiphase Flows with Droplets and Particles. CRC Press.
Feng, Z., Michaelides, E.E., 2005. Proteus: a direct forcing method in the simulations of particulate flows. J. Comput. Phys. 202, 20–51.
Glowinski, R., Pan, T.-W., Periaux, J., 1994a. A fictitious domain method for Dirichlet problems and applications. Comput. Methods Appl. Mech. Eng. 111, 283–303.
Glowinski, R., Pan, T.-W., Periaux, J., 1994b. A fictitious domain method for external incompressible viscous flow modeled by Navier–Stokes equations. Comput. Methods Appl. Mech. Eng. 112, 133–148.
Glowinski, R., Pan, T.-W., Periaux, J., 1995. A Lagrange multiplier/fictitious domain method for the Dirichlet problem Generalization to some flow problems. Jpn. J. Ind. Appl. Math. 12, 87–108.
Glowinski, R., Pan, T.-W., Periaux, J., 1997. A Lagrange multiplier/fictitious domain method for the numerical simulation of incompressible viscous flow around moving rigid bodies (I): the case where the rigid body motions are known a priori. CR Acad. Sci. Paris 324, 361–369.
Glowinski, R., Pan, T.-W., Hesla, T.I., Joseph, D.D., 1999. A distributed Lagrange multiplier/fictitious domain method for particulate flows. Int. J. Multiphase Flow 25, 755–794.
Glowinski, R., Pan, T.-W., Hesla, T.I., Joseph, D.D., Periaux, J., 2001. A fictitious domain approach to the direct numerical simulation of incompressible viscous flow past moving rigid bodies: application to particulate flow. J. Comput. Phys. 169, 363–426.
Happel, J., Brenner, H., 1965. Low Reynolds Number Hydrodynamics. Prentice-Hall, New York.
Höfler, K., Schwarzer, S., 2000. Navier–Stokes simulation with constraint forces: finite-difference method for particle-laden flows and complex geometries. Phys. Rev. E 61, 7146–7160.
Hu, H.H., 1996. Direct simulation of flows of solid–liquid mixture. Int. J. Multiphase Flow 22, 335–352.
Hu, H.H., Joseph, D.D., Crochet, M., 1992. Direct simulation of fluid particle motions. J. Theor. Comput. Fluid Dyn. 3, 285–306.
Hu, H.H., Patankar, A., Zhu, M.Y., 2001. Direct numerical simulations of fluid–solid systems using the arbitrary Lagrangian–Eulerian technique. J. Comput. Phys. 169, 427–462.
Hwang, W.R., Hulsen, M.A., 2006. Direct numerical simulations of hard particle suspensions in planar elongational flow. J. Non-Newtonian Fluid Mech. 136, 167–178.
Hwang, W.R., Hulsen, M.A., Meijer, H.E.H., 2004. Direct simulations of particle suspensions in a viscoelastic fluid in sliding bi-periodic frames. J. Non-Newtonian Fluid Mech. 121, 15–33.
Hwang, W.R., Peters, G.W.M., Hulsen, M.A., Meijer, H.E.H., 2006. Modeling of flow-induced crystallization of particle-filled polymers. Macromolecules 39, 8389–8398.
Johnson, A., Tezduyar, T.E., 1996. Simulation of multiple spheres falling in a liquid-filled tube. Comput. Methods Appl. Mech. Eng. 134, 351–373.
Joseph, D.D., 2002. Interrogations of Direct Numerical Simulation of Solid–Liquid Flow. Online Book. <http://www.efluids.com/efluids/books/joseph.htm>.

Kadaksham, A.T.J., Singh, P., Aubry, N., 2004. Dielectrophoresis of nanoparticles. Electrophoresis 25, 3625–3632.
Kim, D., Choi, H., 2006. Immersed boundary method for flow around an arbitrarily moving body. J. Comput. Phys. 212, 662–680.
Ladd, A.J.C., 1994. Numerical simulations of particulate suspensions via a discretized Boltzmann equation. Part 1. Theoretical foundation. J. Fluid Mech. 271, 285–309.
Ladd, A.J.C., Verberg, R., 2001. Lattice-Boltzmann simulations of particle-fluid suspensions. J. Stat. Phys. 104, 1191–1251.
Le, D.V., Khoo, B.C., Peraire, J., 2006. An immersed interface method for viscous incompressible flows involving rigid and flexible boundaries. J. Comput. Phys. 220, 109–138.
Lin, J., Shi, X., Yu, Z., 2003. The motion of fibers in an evolving mixing layer. Int. J. Multiphase flow 29, 1355–1372.
Lomholt, S., Maxey, M.R., 2003. Force-coupling method for particulate two-phase flow: Stokes flow. J. Comput. Phys. 184, 381–405.
Lomholt, S., Stenum, B., Maxey, M.R., 2002. Experimental verification of the force coupling method for particulate flows. Int. J. Multiphase Flow 28, 225–246.
Matas, J.-P., Morris, J.F., Guazzelli, E., 2003. Transition to turbulence in particulate pipe flow. Phys. Rev. Lett. 90, 014501.
Matas, J.-P., Morris, J.F., Guazzelli, E., 2004. Inertial migration of rigid spherical particles in Poiseuille flow. J. Fluid Mech. 515, 171–195.
Missirlis, K.A., Assimacopoulos, D., Mitsoulis, E., Chhabra, R.P., 2001. Wall effects for motion of spheres in power-law fluids. J. Non-Newtonian Fluid Mech. 96, 459–471.
Mittal, R., Iaccarino, G., 2005. Immersed boundary methods. Annu. Rev. Fluid Mech. 37, 239–261.
Pan, T.-W., Glowinski, R., 2002. Direct simulation of the motion of neutrally buoyant circular cylinders in plane Poiseuille flow. J. Comput. Phys. 181, 260–279.
Pan, T.-W., Glowinski, R., 2005. Direct simulation of the motion of neutrally buoyant balls in a three-dimensional Poiseuille flow. CR Mecanique 333, 884–895.
Pan, T.-W., Joseph, D.D., Glowinski, R., 2001. Modeling Rayleigh–Taylor instability of a sedimenting suspension of several thousand circular particles in direct numerical simulation. J. Fluid Mech. 434, 23–37.
Pan, T.-W., Joseph, D.D., Bai, R., Glowinski, R., Sarin, V., 2002. Fluidization of 1204 spheres: simulation and experiment. J. Fluid Mech. 451, 169–191.
Pan, T.W., Joseph, D.D., Glowinski, R., 2005. Simulating the dynamics of fluid–ellipsoid interactions. Comput. Struct. 83, 463–478.
Pan, T.-W., Glowinski, R., Hou, S.C., 2007. Direct numerical simulation of pattern formation in a rotating suspension of non-Brownian settling particles in a fully filled cylinder. Comput. Struct. 85, 955–969.
Pan, T.W., Chang, C.C., Glowinski, R., 2008. On the motion of a neutrally buoyant ellipsoid in a three-dimensional Poiseuille flow. Comput. Methods Appl. Mech. Eng. 197, 2198–2209.
Patankar, N.A., 2001. A Formulation for Fast Computations of Rigid Particulate Flows. Technical Report, CTR Annual Research Briefs.
Patankar, N.A., Singh, P., Joseph, D.D., Glowinski, R., Pan, T.W., 2000. A new formulation of the distributed Lagrange multiplier/fictitious domain method for particulate flows. Int. J. Multiphase Flow 26, 1509–1524.
Patankar, N.A., Huang, P.Y., Ko, T., Joseph, D.D., 2001. Lift-of of a single particle in Newtonian and viscoelastic fluids by direct numerical simulation. J. Fluid Mech. 438, 67–100.
Perrin, A., Hu, H.H., 2008. An explicit finite difference scheme with spectral boundary conditions for particulate flows. J. Comput. Phys. 227, 8776–8791.
Peskin, C.S., 2002. The immersed boundary method. Acta Numer. 11, 479–517.
Phan-Thien, N., Tran-Cong, T., Graham, A.L., 1991. Shear flow of periodic arrays of particle clusters: a boundary-element method. J. Fluid Mech. 228, 275–293.
Pringle, C.C.T., Kerswell, R.R., 2007. Asymmetric, helical, and mirror-symmetric traveling waves in pipe flow. Phys. Rev. Lett. 99, 074502.
Qi, D.W., 1999. Lattice Boltzmann simulations of particles in no-zero-Reynolds-number flows. J. Fluid Mech. 385, 41–62.
Shao, X., Yu, Z., Sun, B., 2008. Inertial migration of spherical particles in circular Poiseuille flow at moderately high Reynolds numbers. Phys. Fluids 20, 103307.
Sharma, N., Patankar, N.A., 2004. Direct numerical simulation of the Brownian motion of particles by using fluctuating hydrodynamic equations. J. Comput. Phys. 201, 466–486.
Sharma, N., Patankar, N.A., 2005. A fast computation technique for the direct numerical simulation of rigid particulate flows. J. Comput. Phys. 205, 439–457.
Sierou, A., Brady, J.F., 2001. Accelerated Stokesian dynamics simulations. J. Fluid Mech. 448, 115–146.
Singh, P., Joseph, D.D., 2000. Sedimentation of a sphere near a vertical wall in an Oldroyd-B fluid. J. Non-Newtonian Fluid Mech. 94, 179–203.
Singh, P., Joseph, D.D., 2005. Fluid dynamics of floating particles. J. Fluid Mech. 530, 31–80.
Singh, P., Joseph, D.D., Hesla, T.T., Glowinski, R., Pan, T.-W., 2000. A distributed Lagrange multiplier/fictitious domain method for viscoelastic particulate flows. J. Non-Newtonian Fluid. Mech. 91, 165–188.
Sun, B., Yu, Z., Shao, X., 2009. Inertial migration of a circular particle in nonoscillatory and oscillatory pressure-driven flows at moderately high Reynolds numbers. Fluid Dyn. Res. 41, 055501.
Tanguy, P.A., Bertrand, F., Labie, R., Brito-De La Fuente, E., 1996. Numerical modelling of the mixing of viscoplastic slurries in a twin-blade planetary mixer. Trans. IChemE, Part A 74, 499–504.
Uhlmann, M., 2005. An immersed boundary method with direct forcing for the simulation of particulate flows. J. Comput. Phys. 209, 448–476.
Veeramani, C., Minev, P.D., Nandakumar, K., 2007. A fictitious domain formulation for flows with rigid particles: a non-Lagrange multiplier version. J. Comput. Phys. 224, 867–879.
Wachs, A., 2009. A DEM-DLM/FD method for direct numerical simulation of particulate flows: sedimentation of polygonal isometric particles in a Newtonian fluid with collisions. Comput. Fluids 38, 1608–1628.
Wang, Z., Fan, J., Luo, K., 2008. Combined multi-direct forcing and immersed boundary method for simulating flows with moving particles. Int. J. Multiphase flow 34, 283–302.
Xu, S., Wang, Z.J., 2006. An immersed interface method for simulating the interaction of a fluid with moving boundaries. J. Comput. Phys. 216, 454–493.
Yu, Z., 2005. A DLM/FD method for fluid/flexible-body interactions. J. Comput. Phys. 207, 1–27.
Yu, Z., Shao, X., 2007. A direct-forcing fictitious domain method for particulate flows. J. Comput. Phys. 227, 292–314.
Yu, Z., Wachs, A., 2007. A fictitious domain method for dynamic simulation of particle sedimentation in Bingham fluids. J. Non-Newtonian Fluid Mech. 145, 78–91.
Yu, Z., Phan-Thien, N., Fan, Y., Tanner, R.I., 2002. Viscoelastic mobility problem of a system of particles. J. Non-Newtonian Fluid Mech. 104, 87–124.
Yu, Z., Phan-Thien, N., Tanner, R.I., 2004. Dynamic simulation of sphere motion in a vertical tube. J. Fluid Mech. 518, 61–93.
Yu, Z., Wachs, A., Peysson, Y., 2006a. Numerical simulation of particle sedimentation in shear thinning fluids with a fictitious domain method. J. Non-Newtonian Fluid Mech. 136, 126–139.
Yu, Z., Shao, X., Wachs, A., 2006b. A fictitious domain method for particulate flows with heat transfer. J. Comput. Phys. 217, 424–452.
Yu, Z., Phan-Thien, N., Tanner, R.I., 2007a. Rotation of a spheroid in a Couette flow at moderate Reynolds numbers. Phys. Rev. E 76, 026310.
Yu, Z., Shao, X., Tanner, R.I., 2007b. Dynamic simulation of shear-induced particle migration in a two-dimensional circular Couette device. Chin. J. Chem. Eng. 15, 333–338.
Zhang, Z., Prosperetti, A., 2005. A second-order method for three-dimensional particle simulation. J. Comput. Phys. 210, 292–324.